Technology and Health Care 24 (2016) S767–S776
DOI 10.3233/THC-161206
IOS Press

Automatic optic disc localization and segmentation in retinal images by a line operator and level sets

Fulong Ren[a,b], Wei Li[b], Jinzhu Yang[a,b], Huan Geng[a,b] and Dazhe Zhao[a,b,*]
[a]*School of Information Science & Engineering, Northeastern University, Shenyang, Liaoning, China*
[b]*Key Laboratory of Medical Image Computing of Ministry of Education, Northeastern University, Shenyang, Liaoning, China*

Abstract.
BACKGROUND: Existing methods may fail to locate and segment the optic disc (OD) due to imprecise boundaries, inconsistent image contrast and deceptive edge features in retinal images.
OBJECTIVE: To locate the OD and detect the OD boundary accurately.
METHODS: The method exploits a multi-stage strategy in the detection procedure. Firstly, OD location candidate regions are identified based on high-intensity feature and vessels convergence property. Secondly, a line operator filter for circular brightness feature detection is designed to locate the OD accurately on candidates. Thirdly, an initialized contour is obtained by iterative thresholding and ellipse fitting based on the detected OD position. Finally, a region-based active contour model in a variational level set formulation and ellipse fitting are employed to estimate the OD boundary.
RESULTS: The proposed methodology achieves an accuracy of 98.67% for OD identification and a mean distance to the closest point of 2 pixels in detecting the OD boundary.
CONCLUSION: The results illuminate that the proposed method is effective in the fast, automatic, and accurate localization and boundary detection of the OD. The present work contributes to the more effective evaluation of the OD and realizing automatic screening system for early eye diseases to a large extent.

Keywords: Optic disc localization, optic disc segmentation, retinal images, level set method

1. Introduction

Automatic optic disc (OD) detection is a very vital task in computer-aided eye disease diagnosis system such as diabetic retinopathy (DR) screening system. It's an essential preprocessing step for identifying other retinal structures, like fovea and retinal vasculature [1,2]. Additionally, before identifying the bright lesions such as retinal exudates, the OD region is normally removed [3]. The OD usually has an elliptical shape and appears bright yellow area crossed by the main blood vessel. The OD rim can be divided into two half zones: temporal and nasal side. Compared with temporal side, the nasal side is usually darker because of most of the darker vessels convergence at this end. But on the contrary, the temporal side is a bright region, and usually contains a 'cup' shape area which is mostly regarded as the brightest part in the retinal image. Figure 1 shows the major structures of the retinal image.

*Corresponding author: Dazhe Zhao, School of Information Science & Engineering, Northeastern University, Shenyang, Liaoning, China. Tel.: +86 2483665401; Fax: +86 2483663446; E-mail: zhaodz@neusoft.com.

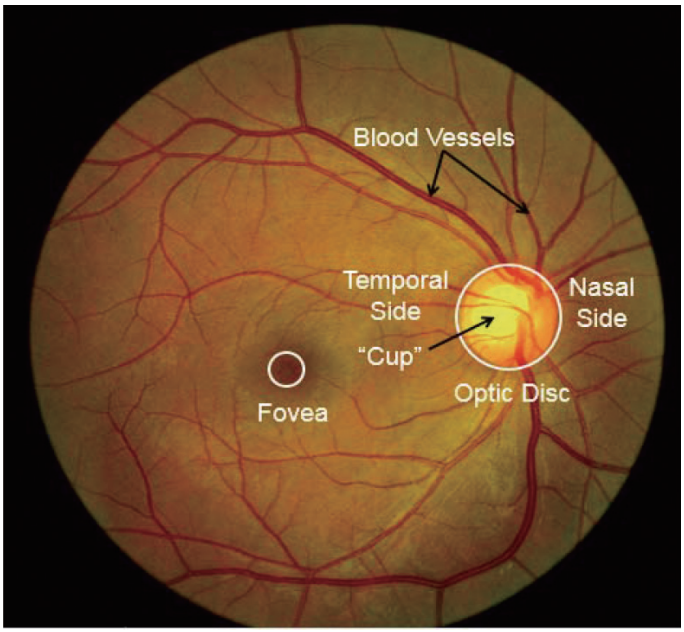

Fig. 1. Retinal image landmarks.

Reliable OD detection is a tremendously difficult matter, since retinal images may suffer from various types of pathological changes and imaging artifacts. A number of studies on OD detection have been reported in literature during recent years. Some research focuses on the brightness and area attribute of the OD [4,5] while some work is based on the vasculature origin and vessel convergence property of the OD [6]. In addition, approaches utilized include exploiting the circular or elliptical shape feature to detect OD [7,8], incorporating multiple attributes of the OD, blending localization techniques and creating a determinative model for the accurate localization of the OD [9,10]. Inspired by previous works, a localization algorithm based on multi-attributes of OD is proposed in this paper. After identifying the OD candidate regions by the OD properties of brightness and vessel convergence respectively, on these candidates an optimized line operator method proposed in [10] is used to locate the OD accurately.

The OD segmentation is a challenging task because of retinal lesion around the disc, uneven illumination, blood vessel hindrance, etc. Among OD segmentation approaches, the level set is one of the most successful and promising methods. In [11], the approximate center of the OD is localized by iterative thresholding, then implicit active contour model is employed to detect exactly the boundary of the OD. A region-based active contour model in a variational level set formulation described in [12] contributes to obtaining desired result in image segmentation even though intensity inhomogeneity occurs in the image. Inspired by the work of [12], this paper presents an algorithm for the accurate OD boundary detection. Iterative thresholding method based on the OD position results in previous localizing, followed by ellipse fitting for achieving an initialized contour. Then, a region-based active contour model in a variational level set formulation based on minimizing a region-scalable fitting (RSF) energy and ellipse fitting again are applied to estimate the OD boundary.

The paper is organized as follows. Section 2 describes the proposed OD localization and boundary segmentation methodology. Experimental results on the images of the MESSIDOR database are then described and discussed in Section 3. Finally, the conclusions of this study are drawn in Section 4.

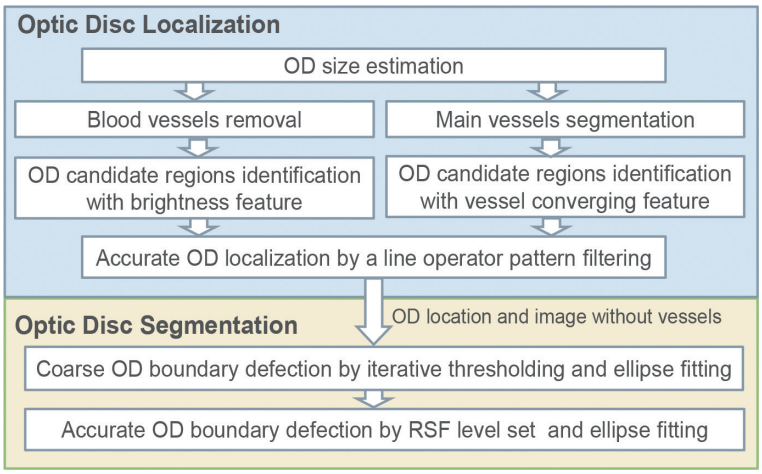

Fig. 2. OD localization and segmentation methodology block diagram.

2. Proposed methodology

The OD localization and segmentation methodology can be schematically described by the block diagram in Fig. 2. The methodology includes two primary processing phases: 1) optic disc localization, for finding a pixel within the disc; 2) optic disc segmentation, for estimating the boundary of the disc. Each phase also consists of several steps and is presented in detail as follows.

2.1. Algorithm for automated OD localization

As a whole OD localization, the algorithm is divided into three successive processing steps: OD size estimation, candidate regions identification and accurate OD localization. The step of candidate regions identification contains two independent procedures based on the OD feature of brightness and vessel convergence separately.

2.1.1. OD size estimation

OD size estimation is the first step of the algorithm, in which values for several important variables used in the subsequent algorithm will be calculated. These variables include the relative OD size, 'cup' size and OD radius, adapted to different image resolutions as well. Similar to [8], the OD radius can be estimated by the field of view (FOV) of the camera, image resolution and the diameter of the average human OD. The image footprint (f_{img}) and imaging area of OD (A_{OD}) are computed as Eqs (1) and (2), respectively.

$$f_{img} = \frac{A_{FOV}}{A_{img\_FOV}} = \frac{A_{OD}}{A_{img\_OD}} \tag{1}$$

$$A_{OD} = \pi \left(D_{OD}/2\right)^2 \tag{2}$$

Where A_{FOV} is the area of the FOV, A_{img_FOV} is the area of the FOV in pixel, A_{img_OD} is the area of the OD in pixel and D_{OD} is the diameter of OD. In this case that the images of MESSIOR database were captured with a 45° FOV, A_{FOV} is approximate to 124.8 mm^2 [13]. Similarly, D_{OD} that is the diameter

of the average human OD has been reported to be approximately 1.85 mm [14]. Therefore, the area of the OD in pixel (A_{img_OD}) and the radius of OD in pixel (R_{img_OD}) can be expressed as Eqs (3) and (4).

$$A_{img\_OD} = \frac{A_{OD}}{f_{img}} = \frac{\pi \left(D_{OD}/2\right)^2}{f_{img}} \tag{3}$$

$$R_{img\_OD} = \sqrt{\frac{A_{img\_OD}}{\pi}} = \sqrt{\frac{\left(D_{OD}/2\right)^2}{f_{img}}} \tag{4}$$

The 'cup' size is often measured in CDR (cup-to-disc ratio) which usually appears below the ratio of 0.65 [15]. Accordingly, the area of the 'cup' in pixel (A_{img_cup}) can be calculated using CDR and it can be defined as Eq. (5).

$$A_{img\_cup} = A_{img\_OD} * CDR \tag{5}$$

As commented, the fundus images from MESSIDOR are 1440 * 960, 2240 * 1488 or 2304 * 1536 pixels in size, corresponding to the OD size (A_{img_OD}) of approximately 13906, 32071 and 35506 pixels, the OD radius (R_{img_OD}) approximately 66, 101 and 106 pixels and the 'cup' size (A_{img_cup}.) of approximately 9039, 20846 and 23080 pixels respectively.

2.1.2. Candidate regions identification

To obtain OD's candidates, the technology based on the brightness feature of OD is described in brief as follows: to extract the areas of pixels having high brightness in different gray levels. The 'cup' is the brightest part of the normal fundus image. Hence its area can be regarded as an identifying criterion and those areas above the criteria are considered as OD's candidates. However before a formal discussion on technique, the vessels should be removed due to the interference to the 'cup' size by outgoing darker vessels. This procedure implicates the image preprocessing with two purposes. One is the noise removal by applying a median filter, the other is the image selection between the red channel in RGB color space and the lightness channel in CIE lab color space. The OD usually appears the most contrast in the red channel compared with other channels in RGB image. Consequently, the red channel image is suitable for the effective detection and segmentation of OD. Unluckily, the saturated phenomenon occurs in some images, which can cause the failure of the relevant algorithm. So the saturation detection of the red channel image is designed based on the gray level values statistics of pixels to solve the issue above. If the average gray level value in FOV is bigger than the 75% of the maximum gray level value (255), the red channel image is assumed to be saturated. In this case, the lightness channel image, which appears high contrast of OD margin and more homogeneous in OD, is selected for further processing.

To remove blood vessels, a set of morphological closing and opening operations using a disc as structuring element, are iteratively applied four times. In this case, the structural element radius of each iteration will decrease to get rid of the different size vessels. Additionally, the initial radius depends on the largest vessels width inside the OD, which is approximately 15% of the OD diameter [16]. The morphological operations are defined as Eq. (6). The vessels are progressively removed. As a result, a clean image will be obtained, simplifying OD candidates' extraction.

$$I_{morph} = \sum_{i=0}^{3} \gamma_{opn}^{B_i}(\varphi_{clo}^{B_i}\left(I_{orig}\right)) \tag{6}$$

Where I_{morph} denotes the resultant image, I_{orig} denotes the original gray scale image, $\varphi_{clo}^{B_i}$ and $\gamma_{opn}^{B_i}$ is are the morphological closing and opening with structuring element B_i, respectively.

An iterative thresholding model is designed to get the candidate(s) OD on the previous image without vessels. In this way, three parameters (maximum grey level, middle grey level and the 'cup' size) are involved in the iteration. The original threshold is initialized with maximum grey level and keeps on decreasing by one level in each iteration while finding the OD candidate(s) using thresholding. In each iteration, the size of each candidate region is compared with the 'cup' size and the one that is greater or equal to the size of 'cup' is considered as an OD candidate. Following this, a minimum bounding rectangle of OD candidate region is obtained as the final OD candidate. To attain the optimal performance, the iteration is broken in the case that the threshold equals to middle grey level or the number of OD candidates reaches six.

Some retinal lesions, such as hard exudates, often produce brighter regions or regions with higher image variation compared with the OD, this case may cause false positives in OD candidate identification based on brightness feature. For this reason, another technology based on vessel converging feature of OD is introduced to obtain OD's candidates. For a start, a method based on the morphological top-hat operation and thresholding is used to segment the main vessels of the retina. A sequential morphological top-hat is iteratively implemented on the green channel image. The selected structural element is a disc whose radius increases for each iteration and the size of the radius goes from half of the largest vessel width to the largest vessel width. The top-hat output in each iteration is accumulated by the supremum operation, a Gaussian filter with 7*7 arithmetic kernel is employed to remove the noise as well. After this, a threshold is selected to apply on the prior output when the resulting mask by thresholding reaches approximately 10% of the FOV area. As a result, a vessel mask is obtained.

Secondly, a rectangular ROI with the size of $2R_{img\_OD}$ * $4R_{img\_OD}$ is used for OD candidate region in the main vessel mask. Furthermore, the two statistic values in the ROI, the mean intensity (M_{ROI}) and the standard deviation of the intensities (σ_{ROI}), are introduced for OD candidate identification. The products of M_{ROI} and σ_{ROI} are sorted in descending order and the ROIs with the values in the top one of the queue are selected as OD candidates.

2.1.3. Accurate OD localization

Up to now, all OD candidates have been obtained and at the next step a method for the optimization of the algorithm proposed in [10] will be used to locate the OD accurately. The algorithm is designed to capture the circular brightness feature associated with OD, tolerant to the retinal lesion and various types of imaging artifacts by the designed line operator as well. A line operator evaluates the image brightness variation along multiple line segments of specific orientations that pass through each retinal image pixel. The orientation of the line segment with the minimum/maximum variation has a specific pattern that can be used to locate the OD accurately. More technical details could be referred to Lu's method [10] and the optimization of the algorithm is described only here. There are three differences compared with the original algorithm in the OD feature detection flow. First, the OD candidate regions with vessels are removed instead of the whole original image as the input of algorithm, which can not only drastically reduce the computational cost with respect to some counterparts, but also improve the accuracy of the defection by less false positive regions. Moreover, another performance improvement is down-sampling applied to reduce the resolution of the input image. However, the size of down-sampling should meet the balance of accuracy and efficiency, here the simple grid sampling with 11*11 is used to gain the best performance. Thirdly, there is scarce macula, which center like the OD center appears a peak in the peak image by a 2-D circular convolution mask, in the OD candidates so that the classification for distinguishing the peak of OD from that of macula has no use for the new optimized flow. More specifically, the correlative position with the maximum score in peak image is identified as the center of OD

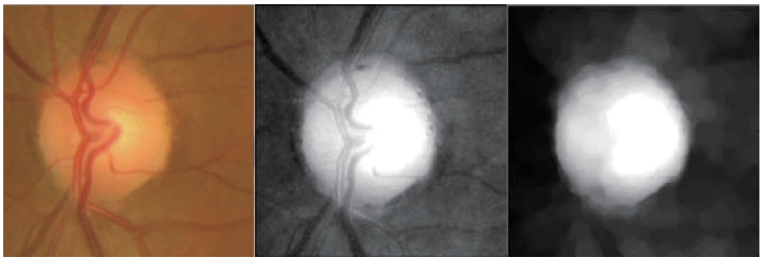

(a) (b) (c)

Fig. 3. Vessel removal based on morphological operation. (a) Original image, (b) the red channel image, (c) vessel removal result.

2.2. Algorithm for automated OD boundary segmentation

The OD boundary segmentation method is composed of two steps: (1) coarse OD boundary defection; (2) accurate OD boundary defection. In the algorithm, the OD location result is inputted as initial information, and the image with the vessels removed mentioned above is regarded as the input image as well. At the first step, a rectangular region is constructed by the size of $4R_{img\_OD}$ * $4R_{img\_OD}$ with this coordinates of OD localization result as its center firstly. To obtain the coarse OD boundary, thresholding method is introduced again. Histogram derived from the defined rectangular region is scanned from the highest intensity value to the lower intensity value. When the result area of thresholding in each scanning is greater than the 'standard' OD area (A_{img_OD}), the scanning is stopped and least square ellipse fitting is employed in the region by thresholding. As a result, a coarse boundary of the OD is obtained. Furthermore, it is taken as the initial contour for the method based on level-set at the next step.

Intensity inhomogeneity and weak boundary partly caused by the vessels removal processing and bad image quality make the accurate OD segmentation tremendous difficult. Fortunately, a region-based active contour model in a variational level set formulation (RSF) can resolve the questions well and also obtain desirable performance. Accordingly, the method, similar to [12], that a RSF model and ellipse fitting are applied to estimate the OD boundary accurately in the next step.

3. Results and discussion

The evaluation of the OD location and segmentation methodology is implemented on the publicly available MESSIDOR database (see http://messidor.crihan.fr, updated 2014 March 13). This database contains 1200 fundus color images of the posterior pole. And 800 of these images were captured with pupil dilation and 400 without dilation, using a Topcon TRC NW6 non-mydriaticretinograph with a 45° FOV. These images were captured at different sizes: 1440*960, 2240*1488 or 2304*1536 pixels and were 8 bits per color plane. Moreover, the "ground truth" for OD boundaries of the 1200 images is publicly available and kindly provided by the University of Huelva, Spain (http://www.uhu.es/retinopathy, updated 2014 May 15) [19].

For the OD detection, if the detected OD lies in the circle of the reference "ground truth", then the localization is deemed successful. The proposed methodology achieves an accuracy of 98.67% by locating correctly 1184 from the 1200 images. Figures 3 and 4 show the indirect results of the proposed method for the OD detection. Figure 5 illustrates the result of the proposed method on normal retina image and kinds of abnormal retina images (detected OD is labeled by "+"). In particular, the three figures

(a) (b) (c)

Fig. 4. OD candidate identification based on vessel convergence. (a) Original image, (b) main vessels mask, (c) OD candidates (white) in the green channel.

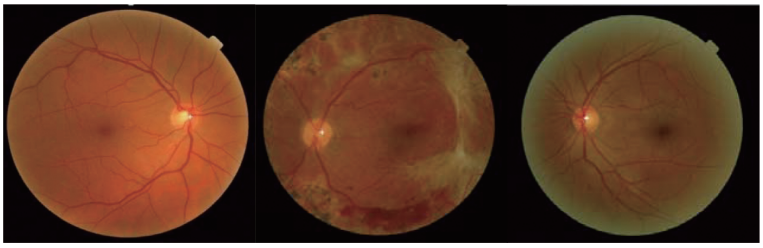

(a) (b) (c)

Fig. 5. OD detection examples: The detected OD is labeled by white "+", (a) The normal image, (b) the lesion image, (c) the artifact image.

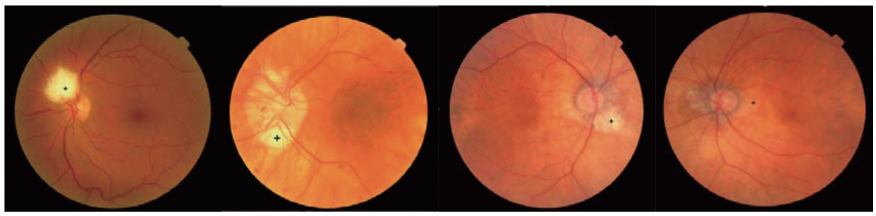

(a) (b) (c) (d)

Fig. 6. OD detection failure examples. The detected OD is labeled by black "+", (a) and (b) failed for the large, bright regions, (c) and (d) failed for the severe lesion making OD dark.

show the normal image, the lesion image and the artifact image, respectively. Despite the existence of dark hemorrhages or bright exudates and pathological regions, the results of the proposed method are satisfactory, and it shows the effectiveness of the proposed method for localizing the center of the optic disc. In Fig. 6, some retinal images with the incorrectly detected optic disc are shown. There are two main factors accounting for the failed OD detection. One is that there is an optic disc-like size region in OD vicinity, which is much brighter than OD (shown in Figs 6(a) and (b)). The other factor is that many severe pathological regions with high number of vessels make OD very blurry, dull and unclassifiable (see Figs 6(c) and (d)).

In view of using grid sampling in the OD detection for the arithmetic efficiency, the size of the grid must be taken into account for the balance of accuracy and efficiency. Table 1 displays a comparison of the accuracies and average time among different sampling widths. The imaging width up-sampling ratios from 5*5 to 17*17 are utilized. The best efficiency appears in 11*11. Our study demonstrates that a lower limit is 5*5, or smaller width could lead the accuracy decreasing to null rapidly.

Table 1
Comparison of different sampling widths

Sampling width[px]	Accuracy	Average time consuming[s/pic]
5*5	82.23	0.24
7*7	94.18	0.39
9*9	96.57	0.61
11*11	98.67	0.73
13*13	98.70	1.14
15*15	98.73	1.23
17*17	98.73	1.56

Table 2
Comparison of OD boundary segmentations using the ratio of MAD over the estimated OD radius

Categories	MAD / R_{img_OD}	H. Yu's	Proposed
Excellent	$\leqslant$ (1/20)	33%	37%
Good	$\leqslant$ (1/10)	68%	66%
Moderate	$\leqslant$ (1/5)	89%	90%
Fair	$\leqslant$ (1/3)	97%	95%

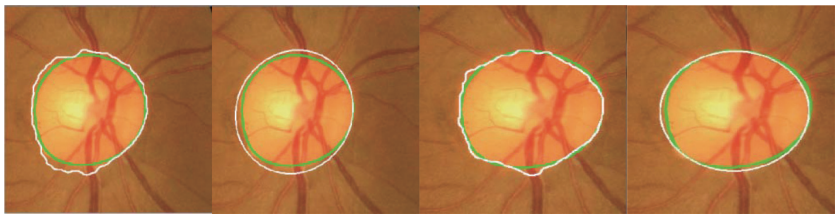

(a) (b) (c) (d)

Fig. 7. OD segmentation (white: segmentation boundary, green: reference standard).

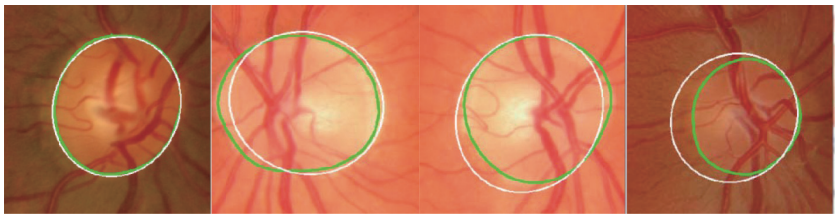

(a) (b) (c) (d)

Fig. 8. Segmentation images in each category (white: segmentation boundary, green: reference standard).

Figure 7 illustrates the indirect results of the proposed method for the OD segmentation. To assess the overall performance of the OD segmentation methods, a common quantitative analysis is performed. This evaluation is based on the similarity in the detected boundary and the detected area respectively. The boundary similarity is evaluated using the average difference between two contours. Define the set of points from the segmented OD boundary as $X = (x_1, x_2, \ldots, x_m)$ and the set of points from the reference standard as $Y = (y_1, y_2, \ldots, y_n)$. For each point in X, its nearest point in Y and their distance is computed as:

$$d_f(x) = \inf\{d(\mathrm{x}, \mathrm{y}) \,|y \in Y\} \tag{7}$$

Where $\inf\{\cdot\}$ represents the infimum and $d(\mathrm{x}, \mathrm{y})$ is the Euclidean distance between x and y. Then, the

Table 3
Percentage of images for each $E_{overlap}$ and M_E

	$E_{overlap} \leqslant 0.05$	$E_{overlap} \leqslant 0.1$	$E_{overlap} \leqslant 0.15$	$E_{overlap} \leqslant 0.2$	$E_{overlap} \leqslant 0.25$	M_E
Proposed	9%	55%	73%	85%	94%	10.8%

self-assessment reliability score is computed as the ratio of the number of x with $d_f(x)$ to the total number of x, and is defined as:

$$E_{score} = \frac{1}{m}\sum_{i=1}^{m} d_f(x) \tag{8}$$

$$MAD = \frac{1}{2}\left[\frac{1}{m}\sum_{i=1}^{m} d_f(x) + \frac{1}{n}\sum_{j=1}^{n} d_f(y)\right] \tag{9}$$

The 500 images chosen randomly from the successful OD localization images and the corresponding "ground truth" boundaries are used for testing. For the optimized results, the coefficients of RSF were slightly tuned, the minimum E_{score} is achieved for $\lambda_1 = \lambda_2 = 1, \mu = 0.07$ and it is approximately 2 pixel. To compare the results obtained by Yu et al. [8] on the same database (MESSIDOR), the ratio of *MAD* (see Eq. (19)) and the estimated OD radius were computed as shown in Table 1. The ratios in Table 2 indicate that the two methods on the overall accuracy have subtle differences, but the proposed method is better than the other one in the higher accurate segmentation. In addition, the test result images are illustrated in Fig. 8. In particular, the four images in the figures show the category of segmentation quality as excellent, good, moderate and fair, respectively.

Another evaluation based on the segmentation area was executed by the overlapping error $E_{overlap}$ as the evaluation metric, and it is defined as:

$$E_{overlap} = 1 - \frac{A_S \bigcap A_G}{A_S \bigcup A_G} \tag{10}$$

Where A_S and A_G denote the area of the segmented OD and the reference "ground truth" respectively. Table 3 shows the test results for the different overlapping errors and the mean overlapping error M_E.

4. Conclusion

This paper presents a novel, automatic, and robust OD localization and segmentation technique. The OD localization methodology tries to exploit synthetically multiple properties of OD (intensity, vessels and shape) to get an optimal result. The methodology exploits not only a relatively simple technique of thresholding based on the 'cup' size, adapted to different image resolutions by using the camera FOV and the image resolution to estimate its area, but also the statistic method based on main vessel to get desired OD candidates. In addition, an optimized flow based on Lu's method can accurately, robustly locate the OD. The initial contour must be as near to the desired boundary as possible for fitting active contour onto the OD. Therefore, the OD segmentation algorithm successively applies thresholding and least square ellipse fitting on a rectangular no-vessels ROI with the OD location as its center, to achieve a rough OD boundary as the initial contour of level set. This step improves not only time efficiency but also accuracy for the next processing based on RSF. Finally, a fast, robust, accurate OD segmentation is achieved by RSF and another ellipse fitting. The present work contributes to the more effective evaluation of the OD and realizing automatic screening system for early eye diseases to a large extent. In the future, a level set model integrated with ellipse shape will be considered to get more reliability and improvement for OD segmentation.

Acknowledgements

This work was partially supported by the National Key Technology Support Program of China (2014BAI17B01) and the National High Technology Research and Development Program of China (2012AA02A607, 2015AA020106).

References

[1] C. Sinthanayothin, J.F. Boyce, H.L. Cook, and T. Williamson. Automatedlocalisation of the optic disc, fovea, and retinal blood vessels fromdigital colour fundus images, Br. J. Ophthalmol, 83 (1999), pp. 902-910.
[2] Li, H., Chutatape, O., Automatic location of optic disc in retinal images, Proc. IEEE Int. Conf. Image Process, 2001, pp. 837-840.
[3] A. Osareh, M. Mirmehdi, B. Thomas, and R. Markham, Automatedidentification of diabetic retinal exudates in digital colour images, Br. J. Ophthalmol, 87 (2003), pp. 1220-1223.
[4] M. Usman Akram, Aftab Khan, Khalid Iqbal and WasiHaider Butt, Retinal Images: Optic Disk Localization and Detection, Computer Science, 6112 (2010), pp. 40-49.
[5] H. Li and O. Chutatape, Automatic location of optic disk in retinal images, in Proc. IEEE-ICIP, 2001, pp. 837-840.
[6] A. Hoover and M. Goldbaum, Locating the optic nerve in a retinalimage using the fuzzy convergence of the blood vessels, IEEE Trans. Med. Imag., 22 (2003), pp. 951-958.
[7] Fleming, A.D., Goatman, K.A., Philip, S., Olson, J.A., Sharp, P.F., Automatic detection of retinal anatomy to assist diabetic retinopathy screening, Phys. Med. Biol., 52 (2007), pp. 331-345.
[8] H. Yu, E.S. Barriga, C. Agurto, S. Echegaray, M.S. Pattichis, W. Bauman, and P. Soliz, Fast localization and segmentation of optic disk in retinal images using directional matched filtering and level sets, IEEE Transactions on Information Technology in Biomedicine, 16 (2012), 644-657.
[9] Touseef Ahmad Qureshi, Hassan Amin, Mahfooz Hussain, Rashid Jalal Qureshi, Bashir Al-Diri, Automatic localization of the optic disc in retinal fundus images using multiple features, Proceedings of the 2012 IEEE 12th International Conference on Bioinformatics & Bioengineering (BIBE), 2012, pp. 488-493.
[10] Shijian Lu and JooHwee Lim, Automatic Optic Disc Detection FromRetinal Images by a Line Operator, IEEE Transactions on Biomedical Engineering, 58 (2011), pp. 88-94.
[11] P.C. Siddalingaswamy, K. GopalakrishnaPrabhu, Automatic localization and boundary detection of optic disc using implicit active contours. Int. J. Comput. Appl., 1 (2010), pp. 1-5.
[12] Chunming Li, Chiu-Yen Kao, John C. Gore, and Zhaohua Ding, Minimization of region-scalable fitting energy for image segmentation, IEEE Transactions onimageprocessing, 17 (2008), pp. 1940-1949.
[13] Area of the Retina Imaged Comparison. [updated 2014 October 20; cited 2015 February 10]. Available: http://www.optos.com/en-us/Professionals/Optometry/Case-Clinical-Studies/.
[14] L.D. Hubbard, R.J. Brothers, W.N. King, L.X. Clegg, R. Klein, L.S. Cooper, A.R. Sharrett, M.D. Davis, and J.W. Cai, Methods for evaluation of retinal microvascular abnormalities associated with hypertension/sclerosis in the atherosclerosis risk in communities study, Ophthalmology, 106 (1999), pp. 2269-2280.
[15] Z. Zhang, J. Liu, W. Kee, N.M. Tan, J.H. Lim, S. Lu, H. Li, Z. Liang, and T.Y. Wong, Neuro-retinal optic cup detection in glaucoma diagnosis, Biomedical Engineering and Informatics (BMEI), 1 (2009), pp. 1-4.
[16] D.J. Cunningham, Cunningham's Text-Book of Anatomy, Oxford Univ. Press, 1981.
[17] A. Osareh, M. Mirmehdi, B. Thomas, and R. Markham, Comparison ofcolour spaces for optic disc localisation in retinal images, International Conference on Pattern Recognition, 1 (2002), pp. 743-746.
[18] Li, C., Xu, C., Gui, C., Fox, M.D., Level set evolution without reinitialization: a new variational formulation, IEEE Computer Society Conference on Computer Vision and Pattern Recognition, 1 (2005), pp. 430-436.
[19] A. Aquino, M.E. Gegundez-Arias, and D. Marin, Detecting the optic discboundary in digital fundus images using morphological, edge detection, and feature extraction techniques, IEEE Trans. Med. Imag., 29 (2010), pp. 1860-1869.